Drug Deliv. and Transl. Res. (2015) 5:146–159
DOI 10.1007/s13346-013-0154-y

RESEARCH ARTICLE

The incorporation of bFGF mediated by heparin into PCL/gelatin composite fiber meshes for guided bone regeneration

Ji-hye Lee · Young Jun Lee · Hyeong-jin Cho · Dong Wan Kim · Heungsoo Shin

Published online: 11 May 2013

Abstract The concept of guided bone regeneration facilitated by barrier membranes has been widely considered to achieve enhanced bone healing in maxillofacial surgery. However, the currently available membranes are limited in their active regulation of cellular activities. In this study, we fabricated polycaprolactone/gelatin composite electrospun nanofibers incorporated with basic fibroblast growth factor (bFGF) to direct bone regeneration. The fibrous morphology was maintained after the crosslinking and subsequent conjugation of heparin. Release of bFGF from electrospun nanofibers without heparin resulted in a spontaneous burst, while the heparin-mediated release of bFGF decreased the burst release in 24 h. The bFGF released from the nanofibers enhanced the proliferation and migration of human mesenchymal stem cells as well as the tubule formation of human umbilical cord blood cells. The subcutaneous implantation of fibers incorporated with bFGF mobilized a large number of cells positive for CD31 and smooth muscle alpha actin within 2 weeks. The effect of the nanofibers incorporated with bFGF on bone regeneration was evaluated on a calvarial critical size defect model. As compared to the mice that received fibers without bFGF, which presented minimal new bone formation (5.36± 3.4 % of the defect), those that received implants of heparinized nanofibers incorporated with 50 or 100 ng/mL bFGF significantly enhanced new bone formation (10.82±2.2 and 17.55±6.08 %). Taken together, our results suggest that the electrospun nanofibers incorporating bFGF have the potential to be used as an advanced membrane that actively enhances bone regeneration.

Keywords Electrospun · Basic fibroblast growth factor · Mesenchymal stem cells · Guided bone regeneration · Growth factor delivery

J.-h. Lee · Y. J. Lee · H.-j. Cho · D. W. Kim · H. Shin
Department of Bioengineering, Hanyang University,
17 Haengdang-dong, Seongdong-gu,
Seoul 133-791, South Korea

H. Shin (✉)
Institute for Bioengineering and Biopharmaceutical
Research and Institute of Aging Society, Hanyang University,
17 Haengdang-dong, Seongdong-gu,
Seoul 133-791, South Korea
e-mail: hshin@hanyang.ac.kr

Introduction

Due to the increasing demand for treatment of large bone defects in maxillofacial and orthopedic surgery, the concept of guided bone regeneration (GBR) has been considered as a potential approach [1, 2]. The successful bone regeneration often relies on the use of membranes that can prevent fibrous tissue in-growth and facilitate bone formation into defect sites. Although various membranes have been developed in laboratories and some have been available for clinical applications, all have specific indications and limitations [3]. For example, an expanded polytetrafluoroethylene membrane is inert and compatible with bone growth, but it is a non-degradable substance that requires removal [4]. Degradable polymers such as collagen and polylactide are also great candidates, but have several drawbacks related to biocompatibility and mechanical properties [5]. In addition, they are limited in providing instructive signals to actively regulate the migration, proliferation, and differentiation of bone-forming cells.

The incorporation of growth factors into membranes may be an alternative strategy to accelerate bone regeneration, since various growth factors such as bone morphogenetic protein-2 and vascular endothelial growth factor have been widely reported to play roles in osteogenesis during bone development [6–8]. Basic fibroblast growth factor (bFGF) is also a well-known cytokine that regulates the proliferation of endothelial cells and fibroblasts, the migration of osteoblasts and cochlear ganglion neurons in mice, and the differentiation of neuroepithelial cells [9–13]. More importantly, bFGF acts

as a strong angiogenesis inducer implicated in enhanced bone repair [14–19]. However, the intravenous administration of bFGF may lead to spontaneous diffusion and early degradation due to its short half-life in blood, which results in insufficient stimulation for regeneration [20, 21]. Therefore, the design and development of delivery vehicles for the local and controlled release of bFGF has been actively pursued. For example, bFGF placed within gelatin microspheres was sandwiched with collagen sponge membranes, which were used in the regeneration of alveolar bone defects [22]. Another study showed that bFGF incorporated into a collagen hydrogel enhanced the proliferation and osteogenic differentiation of rat mesenchymal stem cells (MSCs) [23].

The electrospinning technique has been widely used to fabricate highly porous fibrous meshes for tissue engineering applications [24]. Besides their sufficient porosity and flexibility, electrospun fibers may be prepared to exhibit small pore sizes (in the range of a few micrometers) that selectively allow for nutrient diffusion while inhibiting the penetration of connective tissue, which is important for a GBR membrane [25]. The most important feature of electrospun fibers is their ability to mimic the complex three-dimensional structure of matrix fibrils in native tissue with a high surface area that may serve as a depot to store or liberate instructive molecules [26, 27]. Therefore, bFGF was incorporated onto electrospun fibers by simple physical adsorption, which enhanced the proliferation and sprout extension of human umbilical vein endothelial cells (HUVECs) [28]. An additional study involved the direct electrospinning of bFGF with biodegradable polymers or a dual syringe electrospinning technique to load bFGF onto electrospun fibers [29]. Both of these fiber types released bFGF within 1 to 2 weeks, which enhanced the proliferation, collagen production, and gene expression of the ECMs of bone marrow stem cells. However, to our knowledge, the application of a fibrous membrane incorporated with bFGF specifically for the regeneration of bone has yet to be reported.

In our previous study, we developed polycaprolactone (PCL)/gelatin composite fiber meshes for the sustained delivery of bFGF via heparin to improve therapeutic angiogenesis [30, 31]. The results showed that the sustained release of bFGF from heparinized PCL/gelatin composite fiber meshes enhanced the proliferation of HUVECs and human MSCs (hMSCs) as well as in vivo angiogenesis in nude mice. Heparin, the highly negative sulfated glycosaminoglycan, can provide binding moieties for the stabilization and sustained release of growth factors [32]. Heparin can mediate growth factor delivery by acting as an anchoring molecule for growth factors, enabling them to diffuse out in a sustained manner with structure and bioactivity stabilization [10, 33, 34]. With all these, the objectives of this study are: (1) to evaluate the loading efficiency and initial release amount of bFGF from heparinized PCL/gelatin composite fiber meshes, (2) to investigate the effect of bFGF released from the fiber meshes on the proliferation and chemoattraction of hMSCs and the tubule formation of HUVECs, (3) to analyze the effect of bFGF incorporated into fiber meshes on angiogenesis after subcutaneous implantation, and (4) to investigate its effect on bone regeneration in a mouse calvarial critical size defect (CSD) model.

Experimental part

Materials

PCL (M_w=80,000), gelatin type B (from bovine skin), 2-(*N*-morpholino)ethanesulfonic acid (MES) sodium salt, 1-ethyl-3-(3-dimethylaminopropyl)-1-carbodiimide hydrochloride (EDC), *N*-hydroxysuccinimide (NHS), ethylenediaminetetraacetic acid (EDTA), and polyoxyethylene bisamine (PEG-diamine) were purchased from Sigma-Aldrich (St. Louis, MO, USA). Genipin and 1,1,1,3,3,3-hexafluoro-2-propanol (HFP) were purchased from Wako Pure Chemical Industries (Chuo-ku, Osaka, Japan). Heparin sodium salt was purchased from Acros Organics (Geel, Belgium), and bFGF and a bFGF ELISA development kit were purchased from Peprotech (Rocky Hill, NJ, USA). Dulbecco's modified Eagle's medium (DMEM), Dulbecco's phosphate-buffered saline (PBS), and fetal bovine serum (FBS) were purchased from Gibco BRL (Carlsbad, CA, USA). Endothelial cell basal medium-2 (EBM-2) was purchased from Lonza Group Ltd. (Münchensteinerstrasse, Basel, Switzerland). Sucrose and bovine serum albumin (BSA) were purchased from Amresco (Solon, OH, USA).

Methods

Preparation of PCL/gelatin fibrous matrices with immobilized bFGF

PCL and gelatin were dissolved in HFP by stirring with 4 % (*w*/*v*) concentrations for each. The 10 mL of mixed solution was placed in a syringe with a stainless needle and electrospun to the collector (flow rate 1 mL/h, applied voltage 15–20 kV, 25 cm collector distance). The fabricated PCL/gelatin (PG) fiber meshes were dried overnight at room temperature and underwent a crosslinking with 2.0 % (*w*/*v*) genipin in ethyl alcohol (EtOH) for 72 h, and then the remaining genipin was removed by washing several times with EtOH. The crosslinked fibrous meshes were punched into squares (10×10 mm) and immersed in an EDC/NHS solution (0.1 M, pH=5.0, MES buffer) to activate the carboxylic groups. PEG-diamine was then subsequently conjugated for 6 h and rinsed with MES buffer for 12 h. The PEG-diamine-conjugated samples were reacted with activated heparin (10^{-3} M) in the EDC/NHS solution for 3 h and

washed with MES buffer overnight. The prepared samples (PH) were sterilized with 70 % EtOH and UV irradiation for cell culture before immobilization of bFGF. To immobilize the bFGF, the heparinized fibrous meshes were immersed in 500 μL of bFGF solutions (50 or 100 ng/mL bFGF in 0.1 % (*w*/*v*) BSA, 5 % (*w*/*v*) sucrose, and 0.01 % (*w*/*v*) EDTA) with different concentrations for 24 h at room temperature. Sample codes are shown in Table 1. To compare their fiber morphologies, the electrospun fibers were freeze-dried and then examined using scanning electron microscopy (SEM; JEOL, JSM-6300, Tokyo, Japan).

Measurement of bFGF immobilization yield and initial release

After immobilization of bFGF for 24 h, supernatants were collected and the remaining fiber meshes were washed twice with PBS and then incubated in 1 mL of PBS at 37 °C for 24 h to allow the release of bFGF from the fiber meshes. The solutions containing the released bFGF were then collected, and the amounts of immobilized bFGF were indirectly measured using the supernatants. The amounts of bFGF in the collected supernatants and the solutions were determined using the bFGF ELISA kit. The absolute amount of bFGF in the collected supernatants was calculated by substitution into standard curve gradient.

Mitogenic effect of the released bFGF

The hMSCs (Cambrex Inc., Charles City, IA, USA) were used to examine the effect of the bFGF released from the electrospun fiber meshes on cell proliferation. Briefly, the cells were maintained in DMEM supplemented with 10 % FBS and 1 % penicillin/streptomycin under standard culture conditions (37 °C and 5 % CO_2). After the cell density reached 70 % confluency, the cells were enzymatically detached and seeded onto the culture plates at a density of 5×10^3 cells/cm^2 with DMEM containing 2 % FBS and 1 % PS. After 24 h, the transwell inserts (6.5-mm Transwell® with 8.0-μm pore polycarbonate membrane insert; Corning Inc., Tewksbury, MA, USA) were placed on the culture plate after changing to fresh media with the prepared square shape (1×1 cm) fiber meshes to allow the release of bFGF. An WST-1 assay (EZ-Cytox, Itsbio, Seoul, South Korea) was performed after 24 h of culturing to examine the proliferation of the hMSCs. Briefly, the cells were incubated with water-soluble tetrazolium salts for 1 h at 37 °C, and 200 μL of reacted solutions was transferred into a 96-well culture plate. Optical density was detected at 440 nm wavelength, and the values were normalized with the value of the PH group to represent relative proliferation.

Table 1 Sample preparation conditions and sample codes

Sample code	Composition	bFGF conc.[a] (ng/mL)
PH	PCL/gelatin/Hep	0
PH-b50	PCL/gelatin/Hep	50
PH-b100	PCL/gelatin/Hep	100

[a] The concentration of bFGF used for incorporation into heparinized PCL/gelatin fibrous mesh (PCL/gelatin/Hep)

Chemoattraction assay of hMSCs

To examine the chemoattractive effect of the bFGF released from the heparinized fiber meshes, 2×10^4 cells/cm^2 of hMSCs were seeded onto the transwell inserts (0.33 cm^2) with DMEM containing 2 % FBS and 1 % PS. After 24 h, each fibrous mesh was placed in the lower well of a transwell culture plate with changing media to allow cell migration to the underside of the membrane for the transwell insert. The transwell inserts were separated from the culture plates after 24 h of migration. Then, the cells on the upper side of the insert membrane were removed by cotton swabs leaving only the cells that had migrated to the underside. The cells were fixed with 4 % paraformaldehyde for 30 min and stained with hematoxylin for 10 min. The membranes were directly mounted on a slide glass with mounting solution and observed under an optical microscope (Nikon TE 2000, Tokyo, Japan). The stained cells for each group were counted for three regions in each of five samples and normalized with the number of cells for the control group to represent a migrated cell index.

Tubule formation assay of HUVECs on Growth Factor Reduced Matrigel™

The in vitro angiogenic effects were examined by tubule formation assays on Growth Factor Reduced Matrigel™ (BD Biosciences, San Jose, CA, USA). To prepare the Matrigel™ matrix on culture plates, 200 μL of Matrigel™ was added to a pre-chilled 24-well (1.99 cm^2) culture plate after slow thawing and solidified at 37 °C for 1 h. HUVECs were seeded onto a solidified Matrigel™ matrix with EBM (2.5×10^4 cells/cm^2). After 24 h, the prepared fiber meshes were placed on the top of the culture plate within transwell inserts. The tubule formation was observed with a phase-contrast microscope (Olympus CKK 41, Hauppauge, NY, USA) after 17 h of release, and the pictures were taken using a digital camera (Infinity1, Lumenera Corp., Ottawa, ON, Canada). The analysis of tubule formation was automatically performed using Wimtube software (Wimasis, Munich, Germany).

In vivo angiogenesis assay

The angiogenic activity of bFGF from heparinized PG fiber meshes was investigated by subcutaneous implantation in an

animal model. All animal experiments were approved by the Institutional Animal Care and Use Committee of Hanyang University (HY-IACUC 11-017) and followed the guidelines for the care and use of laboratory animals. The prepared fiber meshes were implanted on the dorsal sites of six male Institute of Cancer Research (ICR) mice (6 weeks old, 25 g body weight; Orient Bio, Seoul, South Korea), and all animals were kept in a specific pathogen-free barrier facility. For the study of angiogenesis induced by bFGF from fibers, we prepared four square-shaped fiber meshes (5×5 mm), which were overlaid to each other. The mice were anesthetized with xylazine (10 mg/kg) and zoletil (60 mg/kg), and the four-layered implants were subcutaneously placed into two separate sites per mouse by minimal skin incision and sutured using 6–0 silk sutures (Ethicon, Somerville, NJ, USA). All animals received humane care in compliance with "the Guide for the Care and Use of Laboratory Animals" (NIH publication no. 85-23, revised 1996). After 2 weeks, the mice were sacrificed and their skin samples were harvested and fixed with 10 % neutralized formalin. The tissues underwent a dehydration and paraffination process to make paraffin blocks, and the tissues embedded in paraffin were cut into 10-μm-thick slices. Sectioned tissues were stained with hematoxylin and eosin after deparaffination to observe the cell distributions and rough vessel formations surrounding the implanted fibers. Immunofluorescence staining was performed with sections for anti-smooth muscle α-actin and anti-CD31 to stain the arterioles and capillaries, respectively, near the fibrous matrices. Then, the sections were sequentially reacted with fluorescein isothiocyanate-conjugated secondary antibodies and counterstained with 40,6-diamidino-2-phenylindole. For the quantification of the arterioles and capillaries surrounding the fiber meshes, ten randomly selected fluorescence images of sections per sample were counted under a fluorescence microscope (TE-2000; Nikon Corp.).

Mouse calvarial critical size defect model

For the in vivo bone regeneration test, the samples were implanted into a calvarial critical size defect model of 6-week-old ICR mice. The mice underwent anesthetization with xylazine (20 mg/kg) and zoletil (60 mg/kg), and scalp hair was shaved for head skin incisions. Each cranium was exposed by incision from the middle site of the eyes to the nuchal region after sterilization using 70 % EtOH. Two critical size defects were made on the skull by a 4-mm-diameter surgical trephine bur (Marathon 3 Champion, Foshan Core Deep Medical Apparatus Co., Ltd., China). The fibers were cut into round shape (5 mm in diameter) and implanted onto the right defect only as a GBR membrane, while the left defect was left without fiber implantation as a control group. Then, the surgery region was sutured with suture silk, and the animals were kept for 2 months.

Radiological analysis

The mice were sacrificed using CO_2 gas to analyze bone regeneration at 2 months post-implantation. The mouse skulls with the implanted fibers were extracted and fixed with 10 % neutral formalin at 4 °C immediately after being washed with PBS. To obtain an X-ray image, the skulls were placed on the X-ray cassette and exposed to X-ray irradiation for 90 s at 24 kV and 2 mA. The regenerated bone area was measured by Photoshop CS5 software (Adobe, San Jose, CA, USA) using five different X-ray images for each group with the same threshold value. The micro-CT images were obtained under 80 kV and 124 μA using a Skyscan1172 (Bruker microCT, Belgium).

Histological analysis

The skulls were subject to a decalcification process by a decalcification solution (Rapidcal, BBC Chemical, Stanwood, WA, USA) for histological analysis after the radiological analysis. The skulls were dehydrated and paraffinated for paraffin embedding, and the paraffin blocks were sectioned into 6-μm-thick slices. The sections were deparaffinated and stained with Goldner's trichrome staining method. The images were obtained with a Nikon 2000 microscope.

Statistical analysis

Quantitative values are shown as averages ± the standard deviation of the average, and the data were analyzed with Student's t test or ANOVA. A p value less than 0.05 was considered significant.

Results and discussion

We fabricated PCL/gelatin composite fiber meshes by the electrospinning technique. SEM micrographs showed smooth and homogeneously distributed non-woven fibers without the formation of beads, and the diameters of the fibers ranged from approximately 400 to 700 nm (Fig. 1a). The composite fiber meshes were then crosslinked with a 2 % genipin solution to prevent the collapse and dissolution of the gelatin in aqueous solution. Crosslinking with genipin appeared to slightly increase the diameter of individual fibers and to reduce the pore size. However, the overall structure of the electrospun fibers was maintained (Fig. 1b). In order to incorporate bFGF reversibly onto the electrospun fiber meshes via affinity binding, we chemically conjugated heparin onto the crosslinked fibers. As shown in Fig. 1c, heparinization minimally affected the morphology and structure of the fibers. Genipin has been widely employed for the crosslinking of gelatin or collagen due to its biocompatibility and simple reaction process as compared to EDC/NHS or glutaraldehyde vapor [35–37]. Nonetheless, the

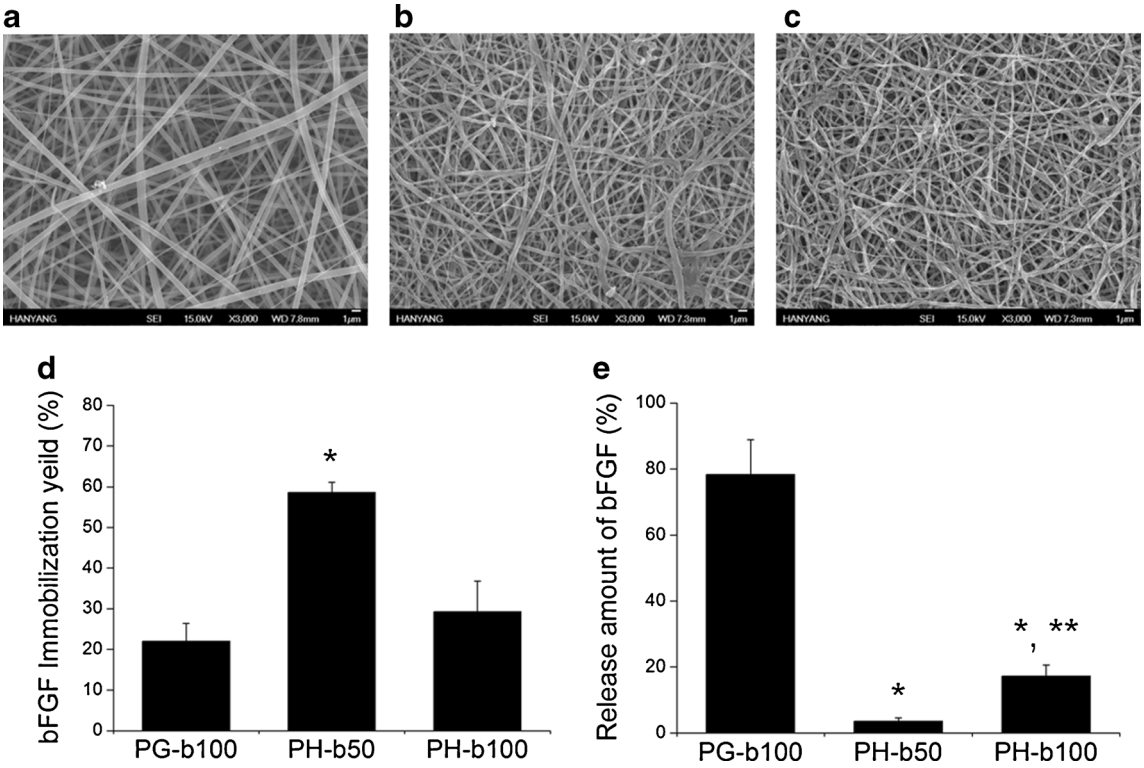

Fig. 1 **a**–**c** SEM images of electrospun fiber meshes: **a** non-crosslinked PG, **b** crosslinked PG, and **c** crosslinked PH. **d**, **e** Characteristics of growth factor immobilization: **d** immobilization yield of bFGF on PG or PH scaffolds; **e** amount of bFGF released from electrospun fiber meshes during the initial 24 h (*, **: $p<0.05$)

optimization of the crosslinking time and concentration of the crosslinker is important to retain the fibrous structure. Our results suggest that the pore size became smaller, which may be attributed to the slight dissolution of gelatin under 99 % EtOH during the crosslinking process. However, the overall fibrous morphology was minimally changed, and the pore size was small enough to prevent migration of connective tissue into the fibers, which was consistent with our previous observations [38].

We then immersed the heparinized PCL/gelatin fibers in the bFGF solution and investigated the effect of heparinization on the immobilization of bFGF using ELISA. Figure 1d shows that approximately 21.95±4.5 % of the bFGF was physically adsorbed on the crosslinked PCL/gelatin fiber meshes without heparinization when reacted with 100 ng/mL of bFGF (PG-b100). In contrast, the immobilization yield of bFGF bound to the heparinized fibers was significantly increased to 58.60± 2.5 % when reacted with 50 ng/mL of bFGF (PH-b50), while the heparinized PG fiber meshes with same concentration (PH-b100) showed a slightly higher immobilization yield (29.25± 7.6 %) than that of PG-b100. The total amount of bFGF was not significantly different when we calculated the incorporated amount of bFGF for each fiber mesh type (data not shown). In our previous study, we showed that the maximum concentration of heparin was 1.0 mM by chemical conjugation onto electrospun PCL/gelatin composite fiber meshes, and this resulted in 24.06±3.01 ng of bFGF incorporation [30]. Therefore, the degree of heparinization may act as a limiting factor for the incorporation of bFGF into the fibers. Next, we measured the release amount of bFGF from prepared fiber meshes for 24 h. Figure 1e shows that 78.24±10.6 % of the bFGF was released within 24 h from the PCL/gelatin fiber meshes where bFGF was physically adsorbed without heparinization, indicating an initial burst release. In contrast, the percentages of bFGF released from PH-b50 and PH-b100 were 3.69±1.0 and 17.37±3.3 %, respectively, indicating that burst release was significantly reduced. These results are consistent with our previous study and others. We demonstrated the sustained release of bFGF from the same type of fibers over the course of 28 days with minimal burst release, and heparin-mediated bFGF delivery was performed in various delivery systems including three-dimensional porous scaffolds, nanoparticles, and hydrogels [30, 39–41].

We then analyzed the bioactivity of the bFGF released from the fiber meshes using several in vitro assays to measure the proliferation and chemoattractive migration of hMSCs and the tubule formation of HUVECs. In order to investigate the effect of the released bFGF on the proliferation of hMSCs, cells were seeded onto a tissue culture plate and allowed to adhere for 24 h, and the fiber meshes were then placed on transwell inserts that were placed on the tops of cell-seeded plates. Figure 2 shows that the relative proliferations of the hMSCs cultured

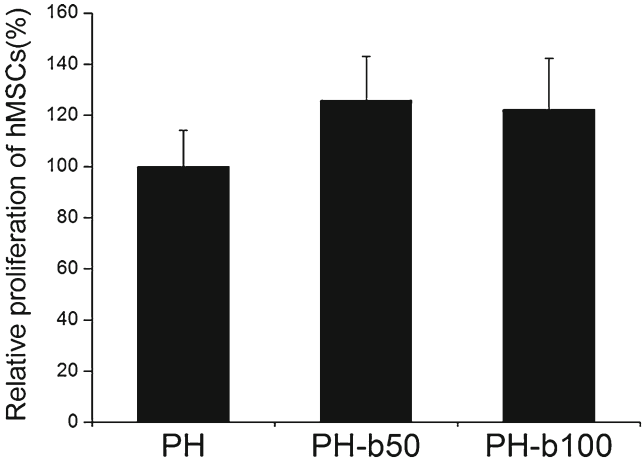

Fig. 2 Effect of bFGF released from the fibrous meshes on the proliferation of MSCs

with the PH-b50 and PH-b100 fibers (fibers incorporated with bFGF) increased to 125.79±17.25 and 122.17±20.1 %, respectively, relative to the group without bFGF. A well-known mitogen, bFGF, is able to enhance the in vitro proliferation of cells such as endothelial cells, fibroblasts, and hMSCs [9, 10, 23, 42]. The mitogenic effect of bFGF is generally proportional to the concentration of the bFGF, but has also exhibited diverse characteristics depending on cell types. For example, Song et al. reported that the treatment of bone marrow mesenchymal stem cells with 5 ng/mL bFGF induced the highest proliferation while those treated with more than 40 ng/mL of bFGF did not show any positive effects on the proliferation for 48 h [42]. Moreover, bFGF incorporated within three-dimensional collagen hydrogels demonstrated similar results in that 5 ng of bFGF/hydrogel resulted in the highest proliferation of hMSCs after 3 days [23]. Our data suggest that bFGF was successfully incorporated in the fiber meshes by heparin and that the concentration of bFGF released from the fiber meshes was within the range that can actively modulate proliferation of hMSCs. These results are also consistent with our previous study, which found that heparin-mediated bFGF delivery was more favorable than bFGF delivery without heparin for the proliferation of HUVECs and hMSCs over 9 days [31].

We then examined the chemoattractive effect of the bFGF released from the electrospun fiber meshes using a transwell system. For this particular experiment, hMSCs were seeded on the transwell insert and the fibers were placed on a tissue culture plate in which the released bFGF could stimulate the migration of hMSCs through the transwell insert. Figure 3 shows that minimal migration of hMSCs through the insert membrane was observed in the control group (no bFGF), which was similar to the group in which hMSCs were exposed to the fibers without bFGF. The migration indices for these groups were similar as well, as shown in Fig. 3e (1.00±0.24 and 1.17±0.28 for the control and PH, respectively). In contrast, the migration of hMSCs was significantly facilitated when they were treated with fiber meshes immobilized with bFGF. The migration indices for PH-b50 and PH-b100 were 3.26±0.85 and 1.97±0.83, respectively. bFGF is highly implicated in the recruitment of endothelial progenitors, which are critical for neovessel formation, and its chemotactic property toward osteogenic cells and MSCs has also been studied [11, 43, 44]. Gawaz et al. showed that the enhanced migration of MSCs by platelet-derived bFGF was blocked by pre-incubation with bFGF antibody, indicating that bFGF is an inducer of migration for MSCs. Our results suggest that the released bFGF retained its chemoattractive effect on hMSCs. The favorable scenario for bone regeneration by employment of a fibrous membrane incorporated with bFGF is the active homing of stem cells that are capable of being differentiated into bone-forming cells at a later stage. It is unclear why the migration of hMSCs under PH-b100 fibers was retarded compared to that under PH-b50. The concentration-dependent migration of hMSCs may require further investigation.

The activity of bFGF released from fiber meshes was also confirmed by the examination of tubule formation of HUVECs cultured on Growth Factor Reduced Matrigel™ (GFR-matrigel). Similar to the proliferation assay of hMSCs, HUVECs were seeded on the GFR-matrigel, and bFGF was allowed to release from fiber meshes through transwell inserts overlaid on cell culture plates. As shown in Fig. 4a, HUVECs were adhered, but showed no indication of tubule formation on the GFR-matrigel and basal media (EBM) that were deprived of the growth factors and supplements essential for tubule formation by HUVECs. In particular, bFGF is crucial in the tubule formation of HUVECs, and the absence of bFGF limits the metabolic activities of HUVECs including spreading and proliferation [31, 41]. Similarly, HUVECs exposed to fiber meshes without bFGF exhibited no tubule formation (Fig. 4b). In contrast, the cells were connected and formed similar numbers of tubules and capillary-like HUVEC networks when exposed to PH-b50 and PH-b100, but the connections between cells appeared to be stronger in the PH-b100 group. To quantify tubule formation, we measured the numbers and total lengths of tubes for each group (Fig. 4b, c). The numbers of tubules were 12.0±2.7 and 13.7±1.5 for the control and PH groups, respectively, while the values significantly increased to 34.0±13.5 and 27.3±7.6 in the PH-b50 and PH-b100 groups, respectively. Furthermore, the total tube lengths were 533.3±87.9 and 528.3±115.5 px for the control and PH groups, respectively, and were significantly enhanced to 1,941.0±931.9 and 1,446.3±550.6 px for PH-b50 and PH-b100, respectively. Quantitative analysis of tubule formation suggests that the bFGF from the fiber meshes was released and significantly enhanced the tubule formation of the HUVECs. The enhanced tubule formation of HUVECs on the GFR-matrigel by bFGF released from heparinized chitosan/poly(γ-glutamic acid) nanoparticles was previously reported and is consistent with our results [41]. Collectively, serial investigations of the in vitro activity of bFGF incorporated

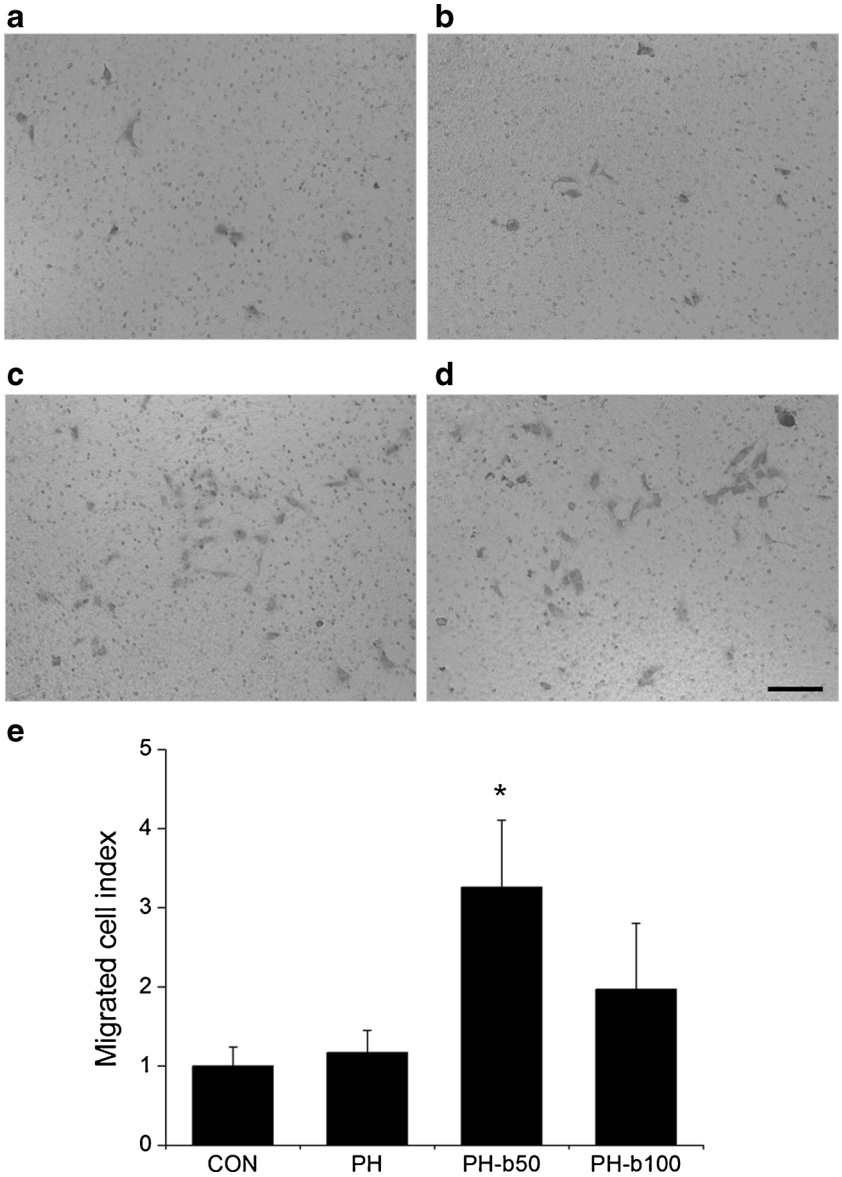

Fig. 3 Chemoattraction assay images of hMSCs after 24 h: **a** control, **b** PH, **c** PH-b50, and **d** PH-b100 (*scale bar*=100 μm). **e** Quantitative results of chemoattraction assay (*$p<0.05$)

into fiber meshes demonstrated that bFGF liberated from the heparinized fiber meshes retained sufficient biological activity to enhance the proliferation and migration of hMSCs as well as the tubule formation of HUVECs. However, the effect of bFGF concentration in the fibers seemed to be insignificant in each experiment, which may require clarification in the future.

Next, we evaluated the effect of bFGF incorporated into fiber meshes on angiogenesis and bone regeneration using animal models. To study in vivo angiogenesis, each fiber was subcutaneously implanted on the dorsal site of mice and retrieved 2 weeks post-surgery. Photographic images show that the implantation of fibers without bFGF did not result in the formation of capillaries on the surface of the fibers or surrounding tissue (Fig. 5a) while the implantation of PH-b50 (Fig. 5b) and PH-b100 (Fig. 5c) resulted in enhanced recruitment of small blood vessels from the surrounding tissue toward the site of the implanted fibers. To confirm these results, we performed histological staining of tissues with hematoxylin and eosin. As shown in Fig. 5d, the fiber meshes served as a barrier to impede the migration of cells involved in the inflammation and wound healing processes, indicating minimal infiltration of cells into the fibers, and fibrous tissue was primarily formed on the surface of the fibers. In contrast, small capillaries were observed away from the fibers when we implanted PH-b50 (Fig. 5e). The implantation of PH-b100 led to more cells being recruited on the surface of the fibers, which may be due to the possible chemoattractive characteristics of the bFGF released from the fibers (Fig. 5f). In addition, relatively larger vessels with red blood cells were observed in this particular group.

We performed immunofluorescent staining for smooth muscle alpha actin (SMA) and CD31 to confirm the distribution of vessels and capillaries (Fig. 6). There was minimal positive staining for SMA after the implantation of fibers without bFGF, while representative patterns for the formation of arterioles were

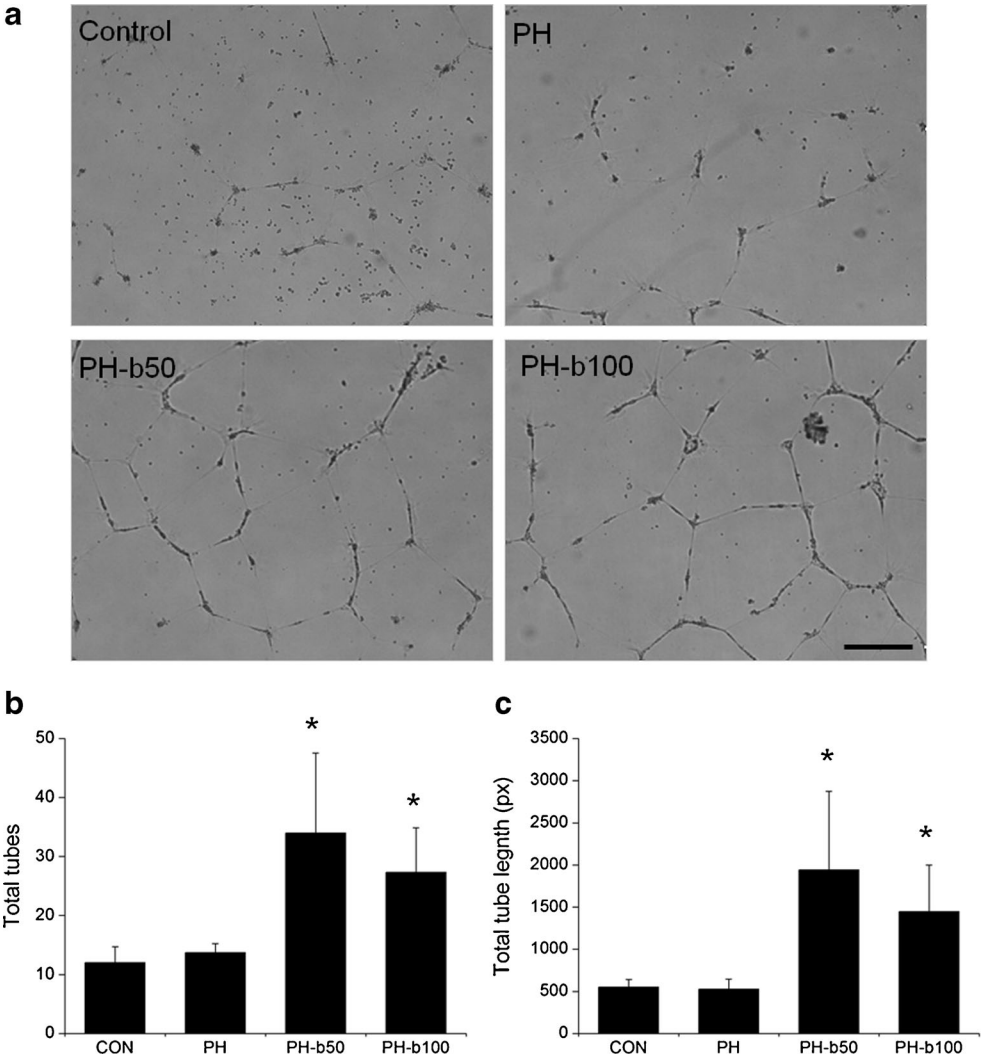

Fig. 4 Tubule formation of HUVECs on GFR-matrigel. **a** Images of HUVECs on GFR-matrigel for each fiber type. *Scale bar*=100 μm. **b** Quantitative results of total tubes; **c** quantitative results of total tube length (*p<0.05)

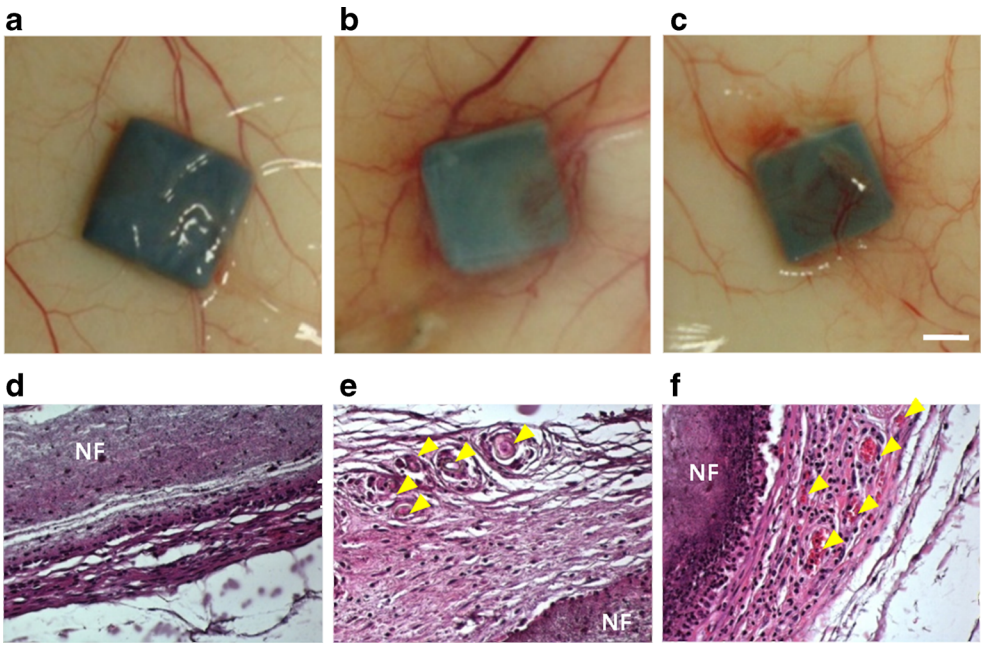

Fig. 5 Analysis of neovascularization after subcutaneous implantation. Photographic images of implanted fiber meshes at 2 weeks post-implantation for **a** PH, **b** PH-b50, and **c** PH-b100. *Scale bar*=2 mm. Histological staining images of implanted fiber meshes with hematoxylin and eosin for **d** PH, **e** PH-b50, and **f** PH-b100. *Arrowhead* = vessel-like structure. *NF* nanofiber. *Scale bar*=50 μm

clearly observed in tissue sections implanted with PH-b50 and PH-b100 fibers after only 2 weeks (Fig. 6a–c). The quantified region positive for SMA significantly increased in PH-b50 and PH-b100 by approximately 4-fold more than that in PH (Fig. 6d). CD31 staining showed that small and vague spots were sparsely observed after the implantation of PH fibers (Fig. 6e) while the lumps of spots that may be considered as immature capillaries were densely observed when PH-b50 and PH-b100 were implanted. The area stained positively for CD31 from the PH-b50 and PH-b100 samples was 3-fold higher than that of PH (Fig. 6h). Several formats of heparin-mediated systems for the delivery of bFGF and their pro-angiogenic activity have been reported in previous literature. Yoon et al. reported a considerable extent of neovascularization after the implantation of pluronic/heparin hydrogels in which 25.2 ng/mg polymer of bFGF was loaded. They showed the angiogenic effect of the hydrogel incorporated with bFGF at 2 weeks after implantation, a similar condition to our system [39]. Another work described injectable heparin-alginate crosslinked gel particles for bFGF stabilization that adsorbed 100 ng of bFGF in 5 mg of heparin–

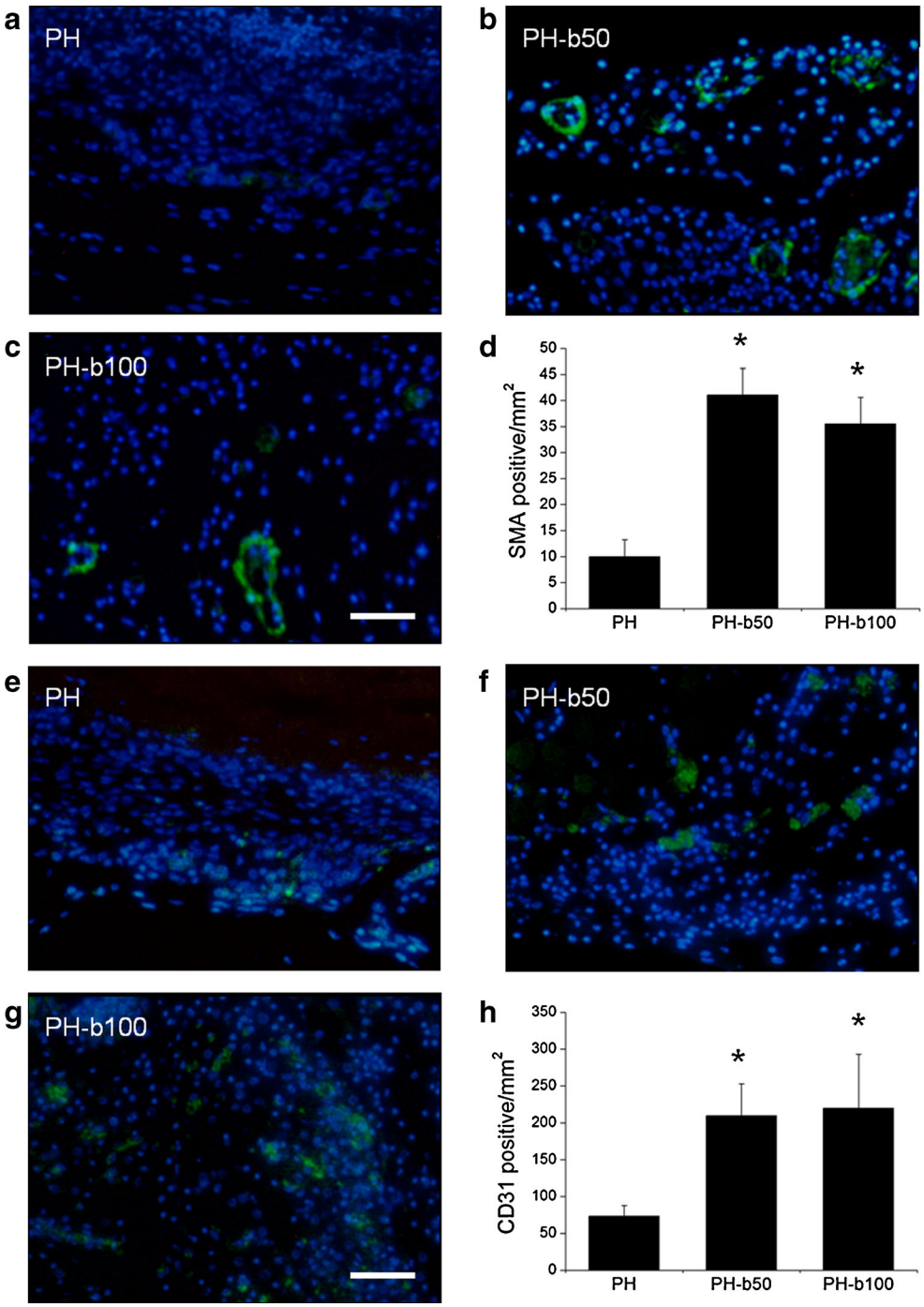

Fig. 6 Immunostaining images of implanted fiber meshes with SMA (**a**–**c**, *green* SMA, *blue* nuclei) and CD31 (**e**–**g**, *green* SMA, *blue* nuclei). *Scale bar*= 50 μm. Quantitative results of **d** SMA and **h** CD31 (*$p<0.05$)

alginate hydrogel and were subcutaneously injected to examine neovascularization [45]. Two weeks after implantation, highly induced neovascularization was observed surrounding the gel particles in the bFGF-adsorbed heparin–alginate hydrogel, but not in the heparin–alginate hydrogels without bFGF or the bFGF-adsorbed alginate hydrogel without heparin. Our previous study also showed the enhanced vessel formation in nude mice by implantation of PCL/gelatin/heparin fiber meshes onto which bFGF had been immobilized [30]. These results demonstrated that heparin-mediated bFGF delivery is favorable for angiogenesis in vivo and the introduction of bFGF into fiber meshes via the simple conjugation of heparin is effective for the stimulation of angiogenesis after subcutaneous implantation.

We then investigated the effect of fiber meshes with immobilized bFGF on in vivo bone regeneration by using the mouse calvarial critical size defect model with a 2-month post-implantation period (Fig. 7). We created two

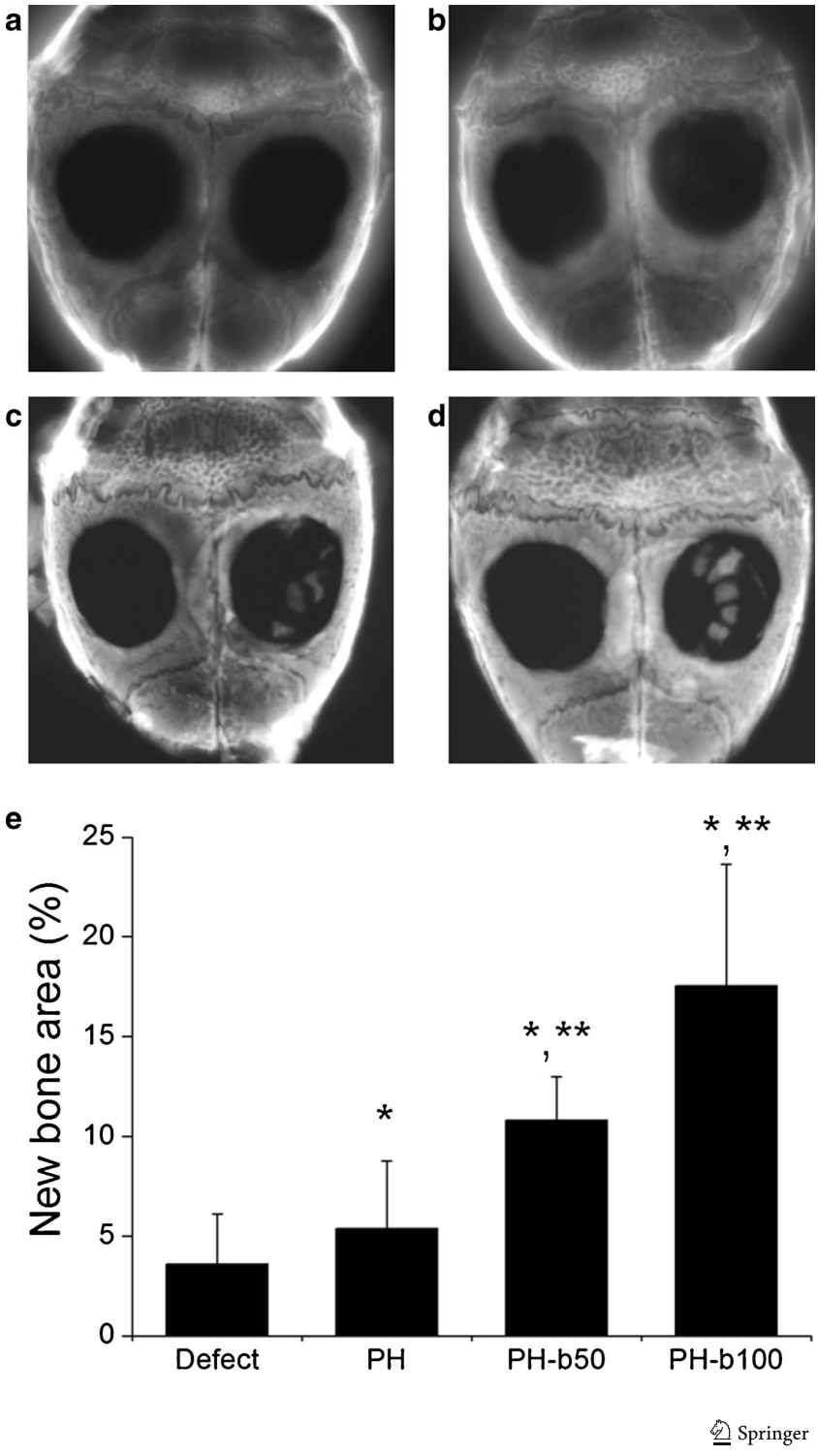

Fig. 7 Soft X-ray images 2 months after the implantation of PH electrospun fibers with immobilized bFGF onto a mouse calvarial critical size defect model. **a** Defect only, **b** PH, **c** PH-b50, and **d** PH-b100. **e** Quantitative results for new bone area (*, **: $p<0.05$)

cranial defects in each mouse, such that all fiber meshes were implanted on the right side and the other defect was left untreated. The CSDs are different from other nonunion models because it is based on the size of the defect; specifically, the CSD-dependent nonunion occurs because the calvarial defect is too large to heal with bony tissue [46]. Since the introduction of the model, CSDs have been used routinely in many laboratories to test the osteogenic capacities of different bone repair techniques. The size of defect was 4 mm diameter for mouse and 8 mm diameter for rat. Especially, making two defects is available for mouse calvarial critical size defect model which is located beside large vessel on their brain and the interval between defects was usually 3~4 mm. A radiological soft X-ray image in Fig. 7a shows that the defect without any treatment has been barely regenerated, indicating that the critical-size defect was successfully generated with very limited spontaneous self-healing. Similarly, the implantation of fibers without bFGF resulted in very weak bone formation at the edge of the bone defect (Fig. 7b). However, the implantation of PH-b50 (Fig. 7c) and PH-b100 (Fig. 7d) fibers enhanced bone regeneration with the formation of relatively large bony islands in the middle of the defects. We then quantified the new bone areas, which were 5.36±3.4 and 3.59±2.5 % for the implantation of PH and the defect without implantation, respectively. In contrast, the implantations of PH-b50 and PH-b100 significantly enhanced bone regeneration up to 10.82±2.2 and 17.55±6.08 %, respectively. Microtomography images re-confirmed these results more clearly, as shown in Fig. 8. The defect and PH groups showed very limited bone regeneration with small bony islands (Fig. 8a, b), while the defect was filled with large pieces of newly grown bone when PH-b50 and PH-b100 fibers were implanted (Fig. 8c, d). Usually, the bone regeneration in defects has been triggered from the edge by the migration of cells from the native bone tissue. Interestingly, the bone regeneration after the implantation of PH-b50 and PH-b100 appeared to occur in the center, rather than edge, of the defects. Although the results are too primitive to make conclusive comments on the exact mechanism behind our observation, our results partially indicate that the incorporation of bFGF may have acted as a chemoattractant to extend the migration of the surrounding cells into the middle of the defect.

To analyze the bone and collagen matrix formation after the implantation of the fiber meshes, the calvarias were cross-sectioned and stained with Goldner's trichrome (Fig. 9). Figures 9a, b shows that thin and loose fibrous tissue was observed in the defect group, and very weak collagen matrix deposition on the remaining fiber meshes was observed after the implantation of PH. Few infiltrated cells were observed inside

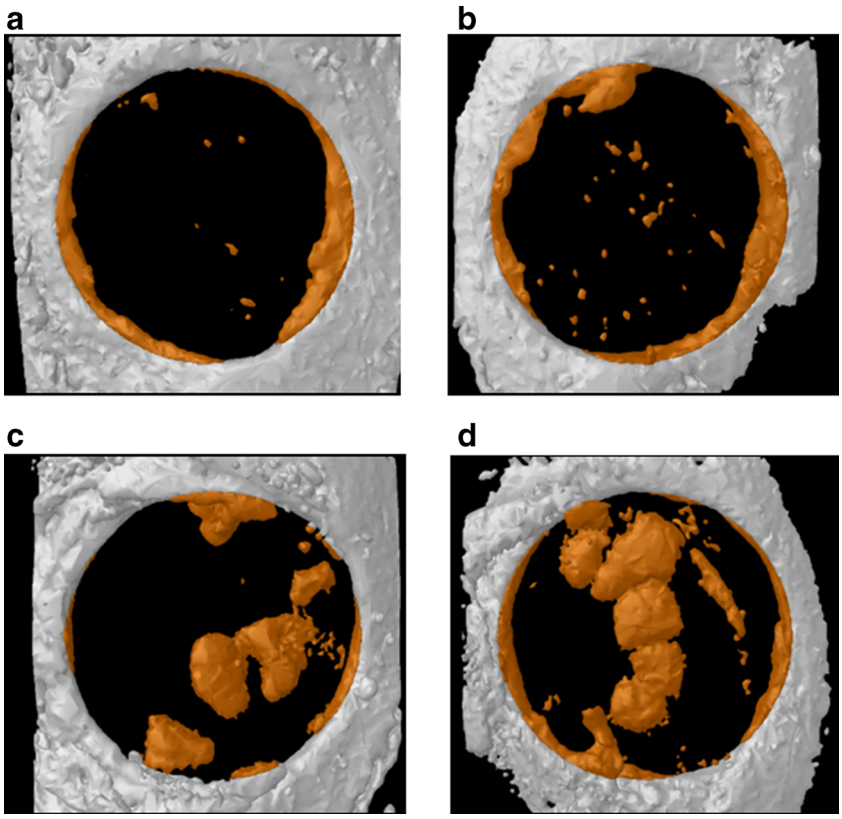

Fig. 8 Images for microtomography of the implantation of electrospun fiber meshes in a mouse calvarial critical size defect model. **a** Defect only, **b** PH, **c** PH-b50, and **d** PH-b100

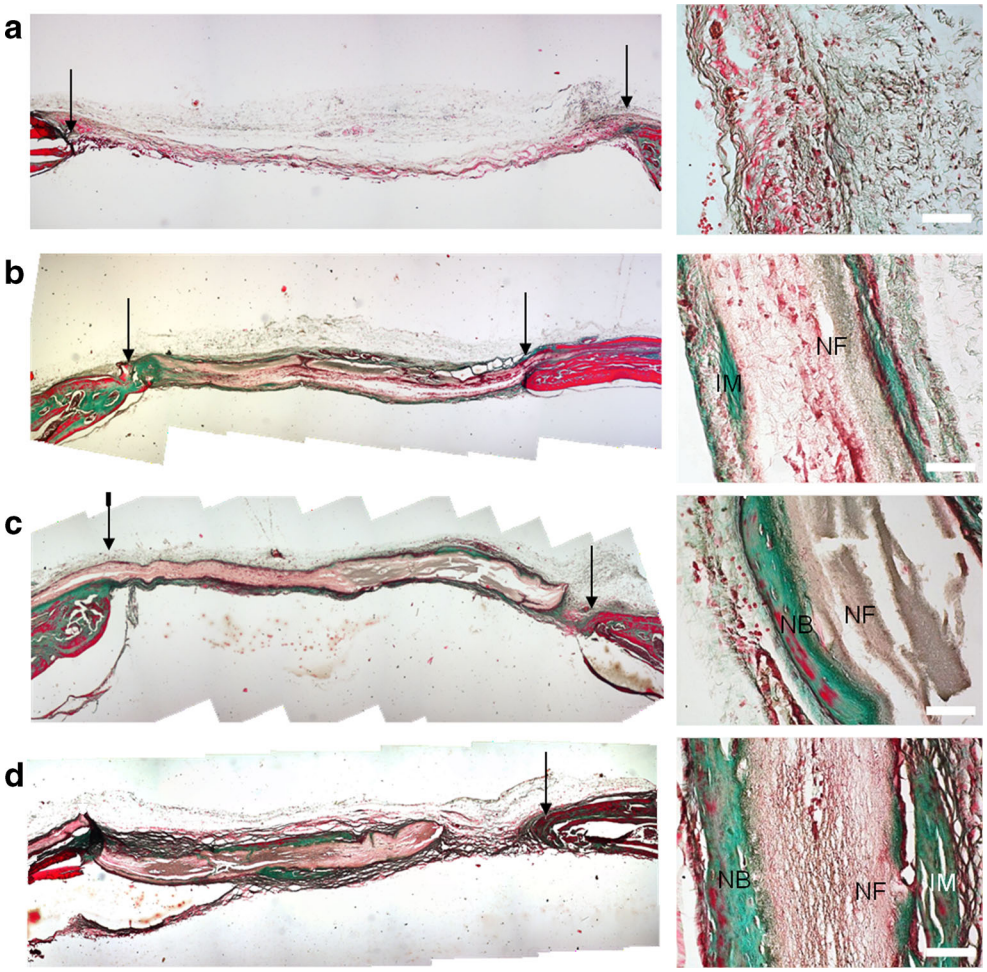

Fig. 9 Images for Goldner's trichrome-stained calvaria at 2 months post-implantation. *Arrows* demonstrate defect sites. **a** Defect only, **b** PH, **c** PH-b50, and **d** PH-b100. *Scale bar*=50 μm. *NB* new bone, *NF* nanofiber, *IM* immature matrix

of the fiber meshes and lining cells were observed on the surface of the fiber meshes (Fig. 9b). After the implantation of PH-b50 and PH-b100, the collagen matrix matured into a bone matrix that possessed bone-specific lacuna structures inside the matrix. In addition, these fibers were retained within the calvarial tissue without severe degradation over 2 months (Fig. 9c, d). These results suggest that the electrospun fiber meshes with immobilized bFGF acted as a guidance membrane to enhance bone regeneration in the calvarial defect model. Many researchers reported the use of materials with immobilized bFGF for bone regeneration. Recombinant bFGF (50 μg/mL) was absorbed onto a disk-type membrane with collagen/nano-bioactive glass, and the bone defect was almost covered with approximately 60 % new bone formation by 3 weeks after implantation [47]. Similarly, gelatin hydrogels incorporated with bFGF were applied to the skull defects of rabbits and resulted in enhanced bone regeneration by regulation of hydrogel degradation, which caused the long-term release of bFGF [21]. Although they achieved enhancement of bone regeneration by the sustained release of bFGF, the amount of bFGF incorporated within the delivery vehicles was quite high (approximately 100 μg). In our results, we showed 17 % of bone regeneration 8 weeks after the implantation of PH-b100, and we anticipate that the improvement in the loading amount of bFGF in the fibrous membrane may facilitate the bone formation with a relatively smaller amount of bFGF. Additional question regarding the release of bFGF is the involvement of enzymes to cleave heparin and thereby regulating release kinetics of bFGF. Although heparin-mediated bFGF delivery system uses affinity binding between heparin and heparin binding domain of bFGF and dissociation of bFGF from heparin occurs by reversibility of their electrostatic interactions, the presence of abundant amount of enzymes such as heparinase may accelerate the release of bFGF. Nonetheless, many studies using heparin-mediated growth factor release system reported that heparin-mediated release of growth factors retarded the burst release of growth factors suggesting that degradation of heparin may not be an important issue. Moreover, a heparinized fiber system can be extended to enable the combined delivery of various growth factors to treat complex diseases.

Conclusions

In this study, fiber meshes onto which bFGF was immobilized were successfully fabricated and mediation with heparin controlled the initial burst release of bFGF. The immobilization of bFGF on the electrospun fiber meshes enhanced the proliferation and migration of hMSCs as well as the tubule formation of HUVECs. Moreover, the subcutaneous implantation of electrospun fiber meshes with immobilized bFGF induced in vivo angiogenesis, which was accompanied by the enhanced formation of arterioles and pre-mature capillaries. Furthermore, bFGF incorporated into electrospun fiber meshes effectively enhanced bone regeneration in a mouse calvarial critical size defect model with relatively smaller amounts of bFGF, and the infiltration of cells into fiber meshes was almost prevented. Therefore, electrospun PCL/gelatin fiber meshes incorporated with bFGF can represent an advanced barrier membrane for guided bone regeneration, which has the ability to regulate proper cell behaviors for effective bone regeneration.

Acknowledgments This research was supported by the National Research Foundation of Korea grant funded by the Ministry of Education, Science and Technology (20120005338).

References

1. Hermann JS, Buser D. Guided bone regeneration for dental implants. Curr Opin Periodontol. 1996;3:168–77.
2. Gerbi ME, Pinheiro AL, Marzola C, Limeira Junior Fde A, Ramalho LM, Ponzi EA, et al. Assessment of bone repair associated with the use of organic bovine bone and membrane irradiated at 830 nm. Photomed Laser Surg. 2005;23(4):382–8.
3. Gentile P, Chiono V, Tonda-Turo C, Ferreira AM, Ciardelli G. Polymeric membranes for guided bone regeneration. Biotechnol J. 2011;6(10):1187–97.
4. Simion M, Dahlin C, Blair K, Schenk RK. Effect of different microstructures of e-PTFE membranes on bone regeneration and soft tissue response: a histologic study in canine mandible. Clin Oral Implants Res. 1999;10(2):73–84.
5. Behring J, Junker R, Walboomers XF, Chessnut B, Jansen JA. Toward guided tissue and bone regeneration: morphology, attachment, proliferation, and migration of cells cultured on collagen barrier membranes. A systematic review. Odontol Soc Nippon Dent Univ. 2008;96(1):1–11.
6. Behr B, Sorkin M, Lehnhardt M, Renda A, Longaker MT, Quarto N. A comparative analysis of the osteogenic effects of BMP-2, FGF-2, and VEGFA in a calvarial defect model. Tissue Eng Part A. 2012;18(9–10):1079–86.
7. Hernandez A, Reyes R, Sanchez E, Rodriguez-Evora M, Delgado A, Evora C. In vivo osteogenic response to different ratios of BMP-2 and VEGF released from a biodegradable porous system. J Biomed Mater Res Part A. 2012;100(9):2382–91.
8. Zhang W, Wang X, Wang S, Zhao J, Xu L, Zhu C, et al. The use of injectable sonication-induced silk hydrogel for VEGF(165) and BMP-2 delivery for elevation of the maxillary sinus floor. Biomaterials. 2011;32(35):9415–24. doi:10.1016/j.biomaterials.2011.08.047.
9. Giraux JL, Matou S, Bros A, Tapon-Bretaudiere J, Letourneur D, Fischer AM. Modulation of human endothelial cell proliferation and migration by fucoidan and heparin. Eur J Cell Biol. 1998;77(4):352–9.
10. Perets A, Baruch Y, Weisbuch F, Shoshany G, Neufeld G, Cohen S. Enhancing the vascularization of three-dimensional porous alginate scaffolds by incorporating controlled release basic fibroblast growth factor microspheres. J Biomed Mater Res Part A. 2003;65(4):489–97. doi:10.1002/jbm.a.10542.
11. Lind M, Deleuran B, Thestrup-Pedersen K, Soballe K, Eriksen EF, Bunger C. Chemotaxis of human osteoblasts. APMIS Acta Pathol Microbiol Immunol Scand. 1995;103(2):140–6.
12. Hossain WA, Morest DK. Fibroblast growth factors (FGF-1, FGF-2) promote migration and neurite growth of mouse cochlear ganglion cells in vitro: immunohistochemistry and antibody perturbation. J Neurosci Res. 2000;62(1):40–55.
13. Murphy M, Drago J, Bartlett PF. Fibroblast growth factor stimulates the proliferation and differentiation of neural precursor cells in vitro. J Neurosci Res. 1990;25(4):463–75.
14. Ledoux D, Gannoun-Zaki L, Barritault D. Interactions of FGFs with target cells. Prog Growth Factor Res. 1992;4(2):107–20.
15. Gibran NS, Isik FF, Heimbach DM, Gordon D. Basic fibroblast growth factor in the early human burn wound. J Surg Res. 1994;56(3):226–34.
16. Mayahara H, Ito T, Nagai H, Miyajima H, Tsukuda R, Taketomi S, et al. In vivo stimulation of endosteal bone formation by basic fibroblast growth factor in rats. Growth Factors. 1993;9(1):73–80.
17. Montesano R, Vassalli JD, Baird A, Guillemin R, Orci L. Basic fibroblast growth factor induces angiogenesis in vitro. Proc Natl Acad Sci U S A. 1986;83(19):7297–301.
18. Nakamura T, Hanada K, Tamura M, Shibanushi T, Nigi H, Tagawa M, et al. Stimulation of endosteal bone formation by systemic injections of recombinant basic fibroblast growth factor in rats. Endocrinology. 1995;136(3):1276–84.
19. Nakasa T, Ishida O, Sunagawa T, Nakamae A, Yokota K, Adachi N, et al. Feasibility of prefabricated vascularized bone graft using the combination of FGF-2 and vascular bundle implantation within hydroxyapatite for osteointegration. J Biomed Mater Res Part A. 2008;85(4):1090–5. doi:10.1002/jbm.a.31673.
20. Bikfalvi A, Klein S, Pintucci G, Rifkin DB. Biological roles of fibroblast growth factor-2. Endocr Rev. 1997;18(1):26–45.
21. Tabata Y, Yamada K, Miyamoto S, Nagata I, Kikuchi H, Aoyama I, et al. Bone regeneration by basic fibroblast growth factor complexed with biodegradable hydrogels. Biomaterials. 1998;19(7–9):807–15.
22. Nakahara T, Nakamura T, Kobayashi E, Inoue M, Shigeno K, Tabata Y, et al. Novel approach to regeneration of periodontal tissues based on in situ tissue engineering: effects of controlled release of basic fibroblast growth factor from a sandwich membrane. Tissue Eng. 2003;9(1):153–62. doi:10.1089/107632703762687636.
23. Oh SA, Lee HY, Lee JH, Kim TH, Jang JH, Kim HW, et al. Collagen three-dimensional hydrogel matrix carrying basic fibroblast growth factor for the cultivation of mesenchymal stem cells and osteogenic differentiation. Tissue Eng Part A. 2012;18(9–10):1087–100. doi:10.1089/ten.TEA.2011.0360.
24. Jun I, Jeong S, Shin H. The stimulation of myoblast differentiation by electrically conductive sub-micron fibers. Biomaterials. 2009;30(11):2038–47.
25. Obata A, Hotta T, Wakita T, Ota Y, Kasuga T. Electrospun microfiber meshes of silicon-doped vaterite/poly(lactic acid) hybrid for guided bone regeneration. Acta Biomater. 2010;6(4):1248–57. doi:10.1016/j.actbio.2009.11.013.
26. Li WJ, Laurencin CT, Caterson EJ, Tuan RS, Ko FK. Electrospun nanofibrous structure: a novel scaffold for tissue engineering. J Biomed Mater Res. 2002;60(4):613–21.
27. Casper CL, Yamaguchi N, Kiick KL, Rabolt JF. Functionalizing electrospun fibers with biologically relevant macromolecules. Biomacromolecules. 2005;6(4):1998–2007.

28. Montero RB, Vial X, Nguyen DT, Farhand S, Reardon M, Pham SM, et al. bFGF-containing electrospun gelatin scaffolds with controlled nano-architectural features for directed angiogenesis. Acta Biomater. 2012;8(5):1778–91.
29. Sahoo S, Ang LT, Goh JC, Toh SL. Growth factor delivery through electrospun nanofibers in scaffolds for tissue engineering applications. J Biomed Mater Res Part A. 2010;93(4):1539–50. doi:10.1002/jbm.a.32645.
30. Kim MS, Bhang SH, Yang HS, Rim NG, Jun I, Kim SI, et al. Development of functional fibrous matrices for the controlled release of basic fibroblast growth factor to improve therapeutic angiogenesis. Tissue Eng Part A. 2010;16(10):2999–3010.
31. Kim MS, Shin YM, Lee JH, Kim SI, Nam YS, Shin CS, et al. Release kinetics and in vitro bioactivity of basic fibroblast growth factor: effect of the thickness of fibrous matrices. Macromol Biosci. 2011;11(1):122–30.
32. Sasisekharan R, Ernst S, Venkataraman G. On the regulation of fibroblast growth factor activity by heparin-like glycosaminoglycans. Angiogenesis. 1997;1(1):45–54.
33. Ishibe T, Goto T, Kodama T, Miyazaki T, Kobayashi S, Takahashi T. Bone formation on apatite-coated titanium with incorporated BMP-2/heparin in vivo. Oral Surg Oral Med Oral Pathol Oral Radiol Endod. 2009;108(6):867–75.
34. Jeong SI, Jeon O, Krebs MD, Hill MC, Alsberg E. Biodegradable photo-crosslinked alginate nanofibre scaffolds with tuneable physical properties, cell adhesivity and growth factor release. Eur Cell Mater. 2012;24:331–43.
35. Liang HC, Chang Y, Hsu CK, Lee MH, Sung HW. Effects of crosslinking degree of an acellular biological tissue on its tissue regeneration pattern. Biomaterials. 2004;25(17):3541–52.
36. Chen YS, Chang JY, Cheng CY, Tsai FJ, Yao CH, Liu BS. An in vivo evaluation of a biodegradable genipin-cross-linked gelatin peripheral nerve guide conduit material. Biomaterials. 2005;26(18):3911–8.
37. Yao C-H, Liu B-S, Hsu S-H, Chen Y-S, Tsai C-C. Biocompatibility and biodegradation of a bone composite containing tricalcium phosphate and genipin crosslinked gelatin. J Biomed Mater Res Part A. 2004;69A(4):709–17. doi:10.1002/jbm.a.30045.
38. Kim MS, Jun I, Shin YM, Jang W, Kim SI, Shin H. The development of genipin-crosslinked poly(caprolactone) (PCL)/gelatin nanofibers for tissue engineering applications. Macromol Biosci. 2010;10(1):91–100.
39. Yoon JJ, Chung HJ, Park TG. Photo-crosslinkable and biodegradable pluronic/heparin hydrogels for local and sustained delivery of angiogenic growth factor. J Biomed Mater Res Part A. 2007;83(3):597–605. doi:10.1002/jbm.a.31271.
40. Shen H, Hu X, Yang F, Bei J, Wang S. Cell affinity for bFGF immobilized heparin-containing poly(lactide-co-glycolide) scaffolds. Biomaterials. 2011;32(13):3404–12. doi:10.1016/j.biomaterials.2011.01.037.
41. Tang D-W, Yu S-H, Ho Y-C, Mi F-L, Kuo P-L, Sung H-W. Heparinized chitosan/poly(γ-glutamic acid) nanoparticles for multi-functional delivery of fibroblast growth factor and heparin. Biomaterials. 2010;31(35):9320–32. doi:10.1016/j.biomaterials.2010.08.058.
42. Song G, Ju Y, Soyama H. Growth and proliferation of bone marrow mesenchymal stem cells affected by type I collagen, fibronectin and bFGF. Mater Sci Eng C. 2008;28(8):1467–71. doi:10.1016/j.msec.2008.04.005.
43. Tengood JE, Ridenour R, Brodsky R, Russell AJ, Little SR. Sequential delivery of basic fibroblast growth factor and platelet-derived growth factor for angiogenesis. Tissue Eng Part A. 2011;17(9–10):1181–9. doi:10.1089/ten.TEA.2010.0551.
44. Langer HF, Stellos K, Steingen C, Froihofer A, Schonberger T, Kramer B, et al. Platelet derived bFGF mediates vascular integrative mechanisms of mesenchymal stem cells in vitro. J Mol Cell Cardiol. 2009;47(2):315–25.
45. Chinen N, Tanihara M, Nakagawa M, Shinozaki K, Yamamoto E, Mizushima Y, et al. Action of microparticles of heparin and alginate crosslinked gel when used as injectable artificial matrices to stabilize basic fibroblast growth factor and induce angiogenesis by controlling its release. J Biomed Mater Res Part A. 2003;67(1):61–8.
46. Schmitz JP, Hollinger JO. The critical size defect as an experimental model for craniomandibulofacial nonunions. Clin Orthop Relat Res. 1986;205:299–308.
47. Hong KS, Kim EC, Bang SH, Chung CH, Lee YI, Hyun JK, et al. Bone regeneration by bioactive hybrid membrane containing FGF2 within rat calvarium. J Biomed Mater Res Part A. 2010;94(4):1187–94.